1P5-7

Investigation of noise reduction filters using singular value decomposition for shear wave elastography

Rikuto Suzuki[1 ‡], Ryo Nagaoka[2*], Masaaki Omura[2], and Hideyuki Hasegawa[2]
([1]Graduate School of Science and Engineering, Univ. of Toyama; [2]Faculty of Engineering, Univ. of Toyama)

1. Introduction

Shear wave elastography (SWE) is a medical imaging diagnostic technique to evaluate tissue stiffness[1)]. By measuring tissue deformation induced by push beam and estimating the shear wave velocity from the deformation, the SWE can visualize tissue stiffness, making it useful for the early detection of liver cancer, which exhibits changes in stiffness due to the disease. SWE possesses the advantage of non-invasiveness and is capable of real-time diagnosis. However, its accuracy is dependent on an operator, and significant errors in the estimated shear wave speeds can occur when a noise component is present in the measurement data. Thus, it is imperative to employ a technique for noise reduction.

The noise reduction method using a singular value decomposition (SVD) based filter has been proposed for the SWE[2)]. However, as the previous paper has focused only on the threshold parameter, there are other parameters in SVD that should be considered, and their optimal values vary depending on the data.

Therefore, this study aims to modify the noise reduction filter for SWE by optimizing not only the threshold but also the datasets and their number in SVD.

2. Methods

2.1. Noise reduction filter

2.1.1. Singular value decomposition

Demene et al. successfully removed clutter signals from an ultrafast Doppler datasets by using SVD based filter[3)]. In this study, we apply this method to the 3D particle velocity of the shear wave to remove the noise components. The dataset used in this study is a three-dimensional matrix of size (n_x, n_z, n_t), where n_x, n_z, and n_t are the number of samples in the lateral, depth, and time directions, respectively. When this 3D matrix is transformed into a Casorati matrix, a Casorati matrix $\boldsymbol{S}$ of size $(n_x \times n_t, n_z)$ is obtained. The matrix $\boldsymbol{S}$ can be decomposed into three matrices using SVD as follows:

$$\mathbf{S} = \mathbf{U}\boldsymbol{\Lambda}\,\mathbf{V}^*, \tag{1}$$

where $\mathbf{U}$ and $\mathbf{V}$ are matrices of sizes $(n_x \times n_t, n_x \times n_t)$ and (n_z, n_z), respectively, * stands for the conjugate transpose, and $\boldsymbol{\Lambda}$ is a diagonal matrix of size $(n_x \times n_z, n_t)$ with singular values arranged in descending order. At this point, shear wave components with high spatiotemporal coherence are detected as higher singular values, while the noise components with low spatiotemporal coherence are detected as lower singular values. Therefore, by retaining only specific singular values and replacing the others with zero, the filtered data $\mathbf{S}^f$ can be obtained as follows:

$$\mathbf{S}^f = \mathbf{U}\boldsymbol{\Lambda}^f\mathbf{V}^*, \tag{2}$$

where $\mathbf{S}^f$ is the filtered data and $\boldsymbol{\Lambda}^f$ is the singular value matrix with unwanted components removed. This is the method of noise removal using SVD. As described above, performing SVD requires a two-dimensional matrix to which SVD is applied and a threshold to extract only the shear wave components. Moreover, since the shear wave components are detected based on the spatiotemporal coherence in the depth direction, it is necessary to determine an appropriate value that considers both noise removal and spatial resolution for the depth size of the dataset used in SVD, especially when constructing two-dimensional Young's modulus maps or shear wave velocity distributions later in the study.

2.1.2. Datasets

In the previous research[4)], it was successful to obtain shear wave propagation data in arbitrary directions using a mask image that removes only specific quadrants after performing a 2D Fourier transform on 3D shear wave propagation data at each depth. In this study, we further adopted a mask image that also removes high-frequency components considered as noise. By applying this to all depths and performing singular value decomposition, we designed a filter with the features of an SVD filter, a low-pass filter, and a directional filter. **Figs. 1(a)-(d)** show the shear wave propagation image at a certain depth, the 2D power spectrum of Fig. 1(a), a mask image for removing components propagating to an opposite side and noise, and the image obtained by applying the mask to Fig. 1(b), respectively.

E-mail: ‡ m23c1027@ems.u-toyama.ac.jp,
* nryo@eng.u-toyama.ac.jp

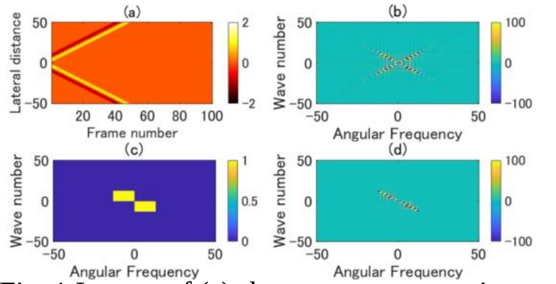

Fig. 1 Images of (a) shear wave propagation, (b) the 2D power spectrum of (a), (c) a mask map for removing components propagating to an opposite side and noise, and (d) a 2D power spectrum obtained by applying the mask.

2.1.3. Threshold

In the previous research[5)], the threshold was determined by the point at which the singular value curve began to flatten. In this study, by applying the approximate linear fitting to the singular value curve, the curve was divided into two segments by a singular value, and the threshold was set at the order of the singular value corresponding to the boundary where the angle between the two lines was minimum.

2.3. Numerical simulations

In this study, the effectiveness of the proposed method was evaluated by performing numerical simulations. The dataset used for the simulations consisted of 3D data simulating the propagation of the shear wave using a sine wave with noise components. In this study, an initial position is the position corresponding to the maximum value at the first frame, and the subsequent positions are estimated from the shift of the shear wave between adjacent frames using the autocorrelation method[6)]. and evaluated by a root mean square error (RMSE) with the true position. The RMSE is calculated as follows:

$$RMSE\ [\%] = \frac{\sqrt{\frac{1}{n_f}\sum_{i=1}^{n_f}|x_{true}(i) - x_{est}(i)|^2}}{\mathrm{mean}(x_{true})}, \quad (3)$$

where x_{true} and x_{est} represent the true and estimated shear wave positions, respectively, and n_f represents the number of frames. In this evaluation, following different conditions were compared; three filter patterns, four noise levels, and ten patterns of sample numbers in the depth direction of the dataset. The filters compared were the proposed method, a method applying singular value decomposition directly to the dataset, and a case without applying any filter. Spike noises were added to 5, 10, 25, and 50% of the pixels in the 2D matrices at each depth, respectively. Additionally, the sample numbers in the depth direction of the dataset were varied from 5, 10, 50, 100, and 150 pixels above and below the reference depth for comparison. The simulations were performed 100 times with different noise pattern, and their average were used for comparison.

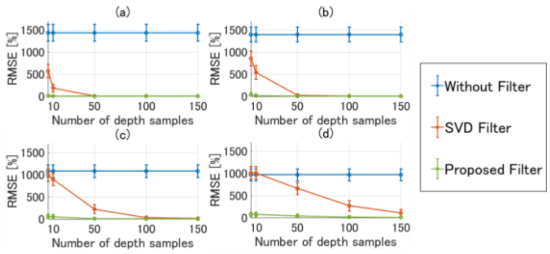

Fig. 2 The RMSEs at each noise level. (a) 5% (b) 10% (c) 25% (d) 50%

3. Results

Figs. 2 (a)-(d) show the results. With 150 depth samples, the RMSEs for the SVD and proposed filters were 2.90% and 2.10% at 5% noise, and 105.32% and 5.93% at 50% noise. This indicates that the proposed filter is better than the conventional SVD filter regardless of the level of the noise components. Additionally, at 5 depth samples and 5% noise, the RMSEs for the SVD and proposed filters were 1010.94% and 69.50%, respectively, so the proposed filter maintained accuracy with fewer depth samples, improving spatial resolution.

4. Conclusion

In this study, we aimed to modify the noise reduction filter for SWE by optimizing not only the threshold but also the datasets and their number in SVD. As a result, the proposed filter was better than the SVD filter in the numerical simulations, and spatial resolution was expected to be improved using the proposed filter.

References

1) J.-L. Gennisson, T. Deffieux, M. Fink, and M. Tanter, Diagn, Interv, Imaging., **94,** 487 (2013).
2) A. Torres, M. L. Palmeri, H. Feltovich, T. J. Hall, and I. M. Rosado-Mendez, Front. Phys. **8**, 606664 (2021)
3) C. Demene, T. Deffieux, M. Pernot, B. F. Osmanski, V. Biran, J. L. Gennisson, L. A. Sieu, A. Bergel, S. Franqui, J. M. Correas, I. Cohen, O. Baud, and M. Tanter, IEEE Trans. Med. Imaging, **34**, 2271 (2015).
4) T. Deffieux, J.-L. Gennisson, J. Bercoff, and M. Tanter, IEEE Trans. Ultrason. Ferroelectr. Freq. Control **58**, 2032 (2011).
5) P. Song, A. Manduca, J. D. Trzasko, and S. Chen, IEEE Trans. Med. Imaging, **36**, 251 (2017).
6) T. C. de Lima, T. S. Pham, X. Ma, H. Tkalčić, Nat. Commun., **14**, 4577 (2023).